Dynamical Mean Field and Dynamical Cluster Approximations

M. Jarrell and A. Macridin

Department of Physics, University of Cincinnati, Cincinnati, Ohio 45221

Abstract. We present a pedagogical discussion of the dynamical mean field and dynamical cluster approximations.

PACS: ...

CONTENTS

1. INTRODUCTION

Some of the most exotic properties of materials, including high-temperature superconductivity, magnetism, and heavy Fermion and non-Fermi liquid behaviors, are due to strong electronic correlations. The materials which display these properties are characterized by either narrow electronic bands or compact orbitals with large angular momentum in the valence shell. In either case, the potential energy associated with some of these electronic degrees of freedom is of similar magnitude or larger than their electronic kinetic energy (bandwidth), which invalidates conventional perturbative approaches. Thus, we resort to the construction of simplified models to study these systems.

For example, the Hubbard model[1] is the simplest model of a correlated electronic lattice system. Both it and the $t-J$ model are thought to at least qualitatively describe some of the properties of transition metal oxides, and high temperature superconductors[2]. The Periodic Anderson model along with various Kondo lat-

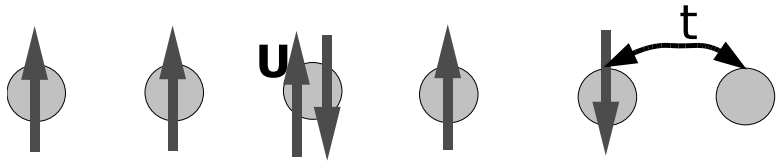

FIGURE 1. Cartoon of the Hubbard model, characterized by a single band with near-neighbor hopping t, and local repulsion U.

tice models have been proposed to describe both the Actinide and Lanthanide Heavy Fermion systems and the Anderson insulators. The Holstein model incorporates the essential physics of strongly interacting electrons and phonons. All of these model Hamiltonians contain at least two major ingredients: a local interaction term and a non-local hopping term. For example, the Hubbard model Hamiltonian is

$$H = -t \sum_{\langle j,k\rangle \sigma} (c^\dagger_{j\sigma} c_{k\sigma} + c^\dagger_{k\sigma} c_{j\sigma}) + \sum_j \varepsilon (n_{j\uparrow} + n_{j\downarrow}) + U(n_{j\uparrow} - 1/2)(n_{j\downarrow} - 1/2)\,, \qquad (1)$$

where $c^\dagger_{j\sigma}$ ($c_{j\sigma}$) creates (destroys) an electron at site j with spin σ, $n_{i\sigma} = c^\dagger_{i\sigma} c_{i\sigma}$, and t sets a unit of energy.

However, except for special limits, even such simplified models like Eq. 1 cannot be solved exactly. For example, for the Hubbard model, no exact solutions exist except in one dimension, where the knowledge is in fact rather complete [3]. The Periodic Anderson model is only solvable in the limit where the orbital degeneracy diverges[4], and the Holstein model is only solvable in the Eliashberg-Migdal limit where vertex corrections may be neglected. Clearly a new approach to these models is needed if nontrivial exact solutions are desired.

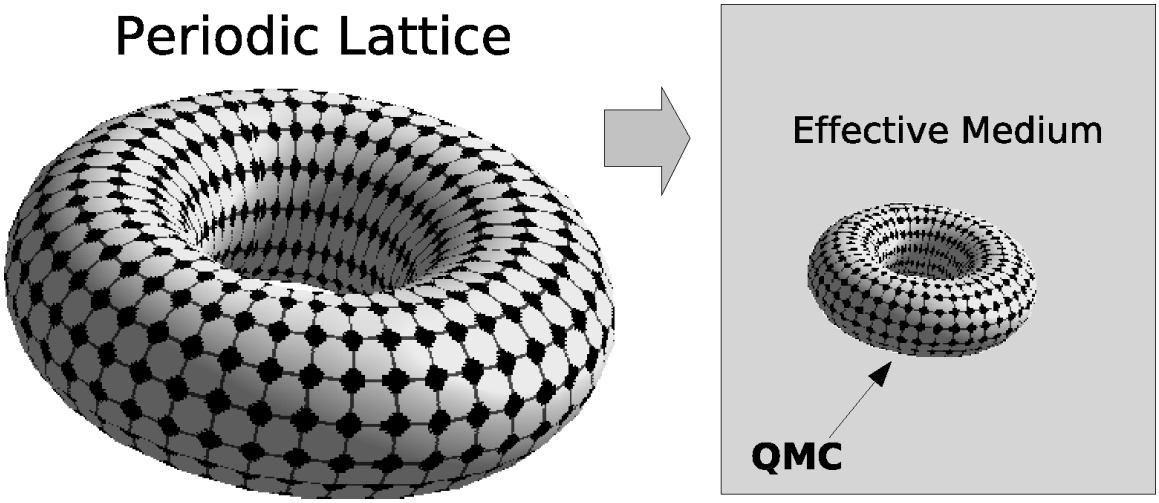

FIGURE 2. Quantum cluster approaches, like the DMFA and DCA, map the infinite lattice problem onto a self-consistently embedded cluster problem.

Metzner and Vollhardt suggested such a new approach [5, 6, 7] based on an expansion in $1/d$ about the point $d = \infty$ to study these strongly correlated lattice models. The

resulting formalism neglects dynamical intersite correlations while retaining the important local dynamical correlations. The resulting formalism is called *Dynamical Mean Field Approximation* since it may be employed in any dimension, but is only exact on infinite dimensional lattices. In finite dimensions, the Dynamical Cluster Approximation is used to study systematic non-local corrections to the DMFA[8, 9]. Quantum cluster approaches such as the DMFA and DCA work by mapping an infinite periodic lattice onto a self-consistently embedded cluster problem, as illustrated in Fig. 2. Correlations up to the cluster size are treated explicitly, while those at longer length scales are treated in a mean field.

In this article, we will assume that you have some working knowledge of the DMFA. In Sec. 2 we will first rederive the DMFA as a course-graining approximation, and then extend this logic to derive the DCA in Sec. 3. Finally, in Sec. 4 we will describe how physical quantities are calculated in this formalism.

2. THE DYNAMICAL MEAN-FIELD APPROXIMATION

The DMFA is a local approximation which was used by various authors in perturbative calculations as a simplification of the k-summations which render the problem intractable[10]. But it was after the work of Metzner and Vollhardt [5] and Müller-Hartmann [6] who showed that this approximation becomes exact in the limit of infinite dimension that it received extensive attention. In this limit, the spatial dependence of the self-energy disappears, retaining only its variation with time. Please see the reviews by Pruschke *et al*[11] and Georges *et al*[12] for a more extensive treatment.

In this section, we will show that it is possible to re-interpret the DMFA as a course graining approximation. For a two-dimensional lattice, this is equivalent to averaging, or coarse-graining, the Green functions used to calculate the irreducible diagrammatic insertions over the Brillouin zone.

Müller-Hartmann[6] showed that this coarse-graining becomes exact in the limit of infinite-dimensions. For Hubbard-like models, the properties of the bare vertex are completely characterized by the Laue function Δ which expresses the momentum conservation at each vertex. In a conventional diagrammatic approach

$$\begin{aligned}\Delta(\mathbf{k}_1,\mathbf{k}_2,\mathbf{k}_3,\mathbf{k}_4) &= \sum_{\mathbf{r}} \exp\left[i\mathbf{r}\cdot(\mathbf{k}_1+\mathbf{k}_2-\mathbf{k}_3-\mathbf{k}_4)\right] \\ &= N\delta_{\mathbf{k}_1+\mathbf{k}_2,\mathbf{k}_3+\mathbf{k}_4}\end{aligned} \tag{2}$$

where $\mathbf{k}_1$ and $\mathbf{k}_2$ ($\mathbf{k}_3$ and $\mathbf{k}_4$) are the momenta entering (leaving) each vertex through its legs of G. However as the dimensionality $D \to \infty$ Müller-Hartmann showed that the Laue function reduces to[6]

$$\Delta_{D\to\infty}(\mathbf{k}_1,\mathbf{k}_2,\mathbf{k}_3,\mathbf{k}_4) = 1 + \mathscr{O}(1/D) \quad . \tag{3}$$

The DMFA assumes the same Laue function, $\Delta_{DMFA}(\mathbf{k}_1,\mathbf{k}_2,\mathbf{k}_3,\mathbf{k}_4) = 1$, even in the context of finite dimensions. More generally, for an electron scatting from an interaction (boson) pictured in Fig. 3, $\Delta_{DMFA}(\mathbf{k}_1,\mathbf{k}_2,\mathbf{k}_3) = 1$. Thus, the conservation of momentum at internal vertices is neglected. We may freely sum over the internal momentum labels

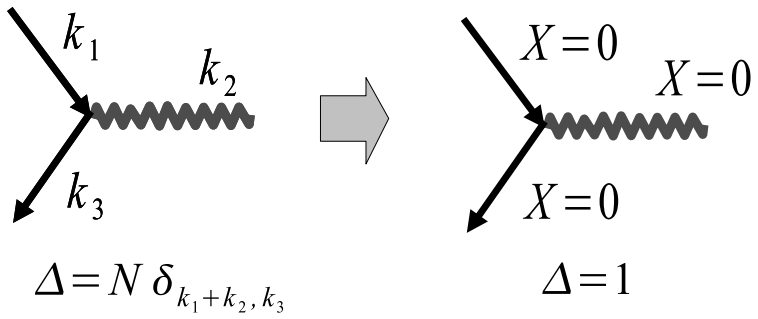

FIGURE 3. The Laue function Δ, which described momentum conservation at a vertex (left). In the DMFA, $\Delta = 1$, so momentum conservation is neglected for compact graphs (right) so that we may freely sum over the momentum labels leaving only local propagators and interactions.

of each Green function leg and interaction leading to a collapse of the momentum dependent contributions leaving only local terms.

This argument may then be applied to the generating functional Φ, which, as illustrated for the second-order contribution in Fig 4, becomes a functional of the local interaction and Green function. The self energy Σ may be obtained from a functional derivative of Φ with respect to the Green function G, which effectively breaks one of the Green function lines.

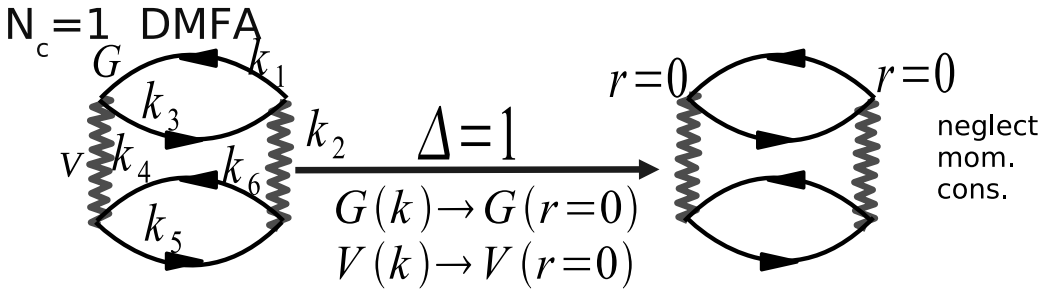

FIGURE 4. The second order contribution the generating functional Φ. As we apply the DMFA coarse-graining approximation, Eq. 3, Φ becomes a functional of the local Green function and interaction.

The perturbative series for Φ, Σ and the irreducible vertices Γ in the DMFA are identical to those of the corresponding impurity model, so that conventional impurity solvers may be used. However, since most impurity solvers can be viewed as methods that sum all the graphs, not just the skeletal ones, it is necessary to exclude $\Sigma(i\omega_n)$ from the bare local propagator $\mathscr{G}$ input to the impurity solver in order to avoid overcounting the local self-energy $\Sigma(i\omega_n)$ ($i\omega_n = (2n+1)\pi T$ is the Matsubara frequency). $\mathscr{G}(i\omega_n)^{-1} = G(i\omega_n)^{-1} + \Sigma(i\omega_n)$ where $G(i\omega_n)$ is the full local Green function. Hence, in the local approximation, the Hubbard model has the same diagrammatic expansion as an Anderson impurity with a bare local propagator $\mathscr{G}(i\omega_n;\Sigma)$ which is determined self-consistently.

An algorithm constructed from this approximation is the following: (i) An initial guess for $\Sigma(i\omega_n)$ is chosen (usually from perturbation theory). (ii) $\Sigma(i\omega_n)$ is used to calculate

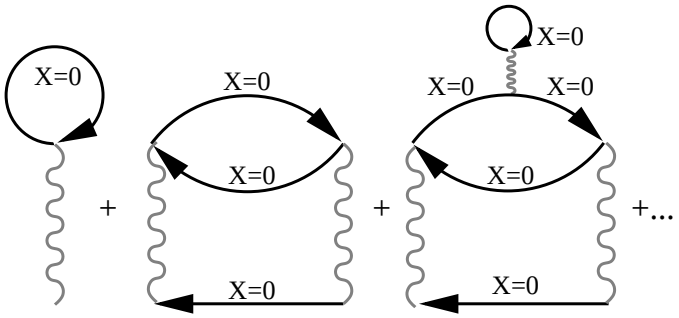

FIGURE 5. The self energy obtained from a functional derivative of the DMFA Φ. Note that it contains local self energy corrections; e.g. in the third graph.

the corresponding local Green function

$$G(i\omega_n) = \int d\eta \frac{\rho^0(\eta)}{i\omega_n - \eta - \varepsilon - \Sigma(i\omega_n)}, \tag{4}$$

where ρ^0 is the non-interacting density of states. (iii) Starting from $G(i\omega_n)$ and $\Sigma(i\omega_n)$ used in the second step, the host Green function $\mathscr{G}(i\omega_n)^{-1} = G(i\omega_n)^{-1} + \Sigma(i\omega_n)$ is calculated which serves as bare Green function of the impurity model. (iv) starting with $\mathscr{G}(i\omega_n)$, the local Green function $G(i\omega_n)$ is obtained using the Quantum Monte Carlo method (or another technique). (v) Using the QMC output for the cluster Green function $G(i\omega_n)$ and the host Green function $\mathscr{G}(i\omega_n)$ from the third step, a new $\Sigma(i\omega_n) = \mathscr{G}(i\omega_n)^{-1} - G(i\omega_n)^{-1}$ is calculated, which is then used in step (ii) to reinitialize the process. Steps (ii) - (v) are repeated until convergence is reached. In step (iv) the QMC algorithm of Hirsch and Fye [13, 14] may be used to compute the local Green function $G(\tau)$ or other physical quantities in imaginary time. Local dynamical quantities are then calculated by analytically continuing the corresponding imaginary-time quantities using the Maximum-Entropy Method (MEM) [15].

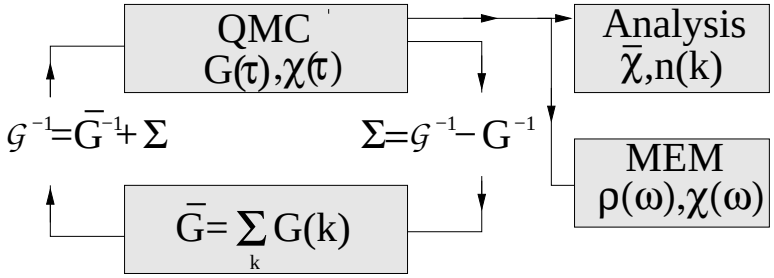

FIGURE 6. The DMFA algorithm. QMC is used as a cluster solver. Once convergence is reached, $G = \bar{G}$, and the irreducible quantities are used in the analysis and Maximum Entropy Method (MEM) codes to calculate the phase diagram and spectra, respectively.

3. THE DYNAMICAL CLUSTER APPROXIMATION

In this section, we will review the formalism which leads to the dynamical cluster approximation. Here, we first motivate the fundamental idea of the DCA which is coarse-graining, we then describe the mapping to an effective cluster problem and discuss the relationship between the cluster and lattice at the one and two-particle level.

3.1. Coarse-Graining

Like the DMFA, the DCA may be intuitively motivated with a coarse-graining transformation. In the DMFA, the propagators used to calculate Φ and its functional derivatives were coarse-grained over the entire Brillouin zone, leading to local (momentum independent) irreducible quantities. In the DCA, we wish to relax this condition, and systematically restore momentum conservation and non-local corrections. Thus, in the DCA, the reciprocal space of the lattice (Fig. 7) which contains N points is divided into N_c cells of identical linear size Δk. The coarse-graining transformation is set by averaging the Green function within each cell. If $N_c = 1$ the original lattice problem is mapped to an impurity problem, and we recover the DMFA. If N_c is larger than one, then non-local corrections of length $\approx \pi/\Delta k$ to the DMFA are introduced. Provided that the propagators are sufficiently weakly momentum dependent, this is a good approximation. If N_c is chosen to be small, the cluster problem can be solved using conventional techniques such as QMC. This averaging process also establishes a relationship between the systems of size N and N_c. A simple and unique choice which will be discussed in Sec. 3.2 is to equate the irreducible quantities (self energy, irreducible vertices) of the cluster to those in the lattice.

3.2. A diagrammatic derivation

This coarse graining procedure and the relationship of the DCA to the DMFA is illustrated by a microscopic diagrammatic derivation of the DCA starting from the Baym generating functional Φ.[19] It is the sum over all closed connected compact graphs constructed from the dressed Green function G and the bare interaction. The self energy Σ_σ is obtained from a functional derivative of Φ, $\Sigma_\sigma = \delta\Phi/\delta G_\sigma$, and the irreducible vetices $\Gamma_{\sigma\sigma'} = \delta\Sigma_\sigma/\delta G'_\sigma$.

The DCA systematically restores the momentum conservation at internal vertices of Φ relinquished by the DMFA. The Brillouin-zone is divided into $N_c = L^D$ cells of size $\Delta k = 2\pi/L$ (c.f. Fig. 7 for $N_c = 8$ and $N_c = 4$). Each cell is represented by a cluster momentum $\mathbf{K}$ in the center of the cell. We require that momentum conservation is (partially) observed for momentum transfers between cells, i.e., for momentum transfers larger than Δk, but neglected for momentum transfers within a cell, i.e., less than Δk. This requirement can be established by using the Laue function [9]

$$\Delta_{DCA}(\mathbf{k}_1, \mathbf{k}_2, \mathbf{k}_3, \mathbf{k}_4) = N_c \delta_{\mathbf{M}(\mathbf{k}_1)+\mathbf{M}(\mathbf{k}_2),\mathbf{M}(\mathbf{k}_3)+\mathbf{M}(\mathbf{k}_4)} \quad , \tag{5}$$

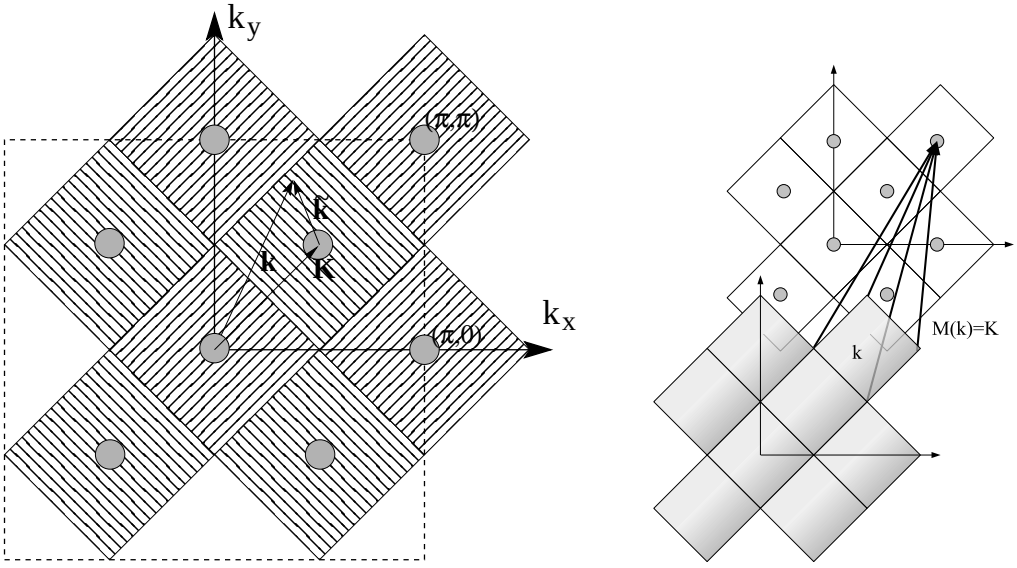

FIGURE 7. (left) Coarse-graining cells for $N_c = 8$ (differentiated by alternating fill patterns) that partition the first Brillouin Zone (dashed line). Each cell is centered on a cluster momentum $\mathbf{K}$ (filled circles). (right) To construct the DCA cluster (e.g. for $N_c = 8$) we map a generic $\mathbf{k}$ to the nearest cluster point $\mathbf{K} = \mathbf{M}(\mathbf{k})$ so that $\tilde{\mathbf{k}} = \mathbf{k} - \mathbf{K}$ remains in the cell around $\mathbf{K}$.

where $\mathbf{M}(\mathbf{k})$ is a function which maps $\mathbf{k}$ onto the momentum label $\mathbf{K}$ of the cell containing $\mathbf{k}$ (see, Fig. 7). This choice for the Laue function systematically interpolates between the exact result, Eq. 3, which it recovers when $N_c \to N$ and the DMFA result, Eq. 3, which it recovers when $N_c = 1$. With this choice of the Laue function the momenta of each internal leg may be freely summed over the cell.

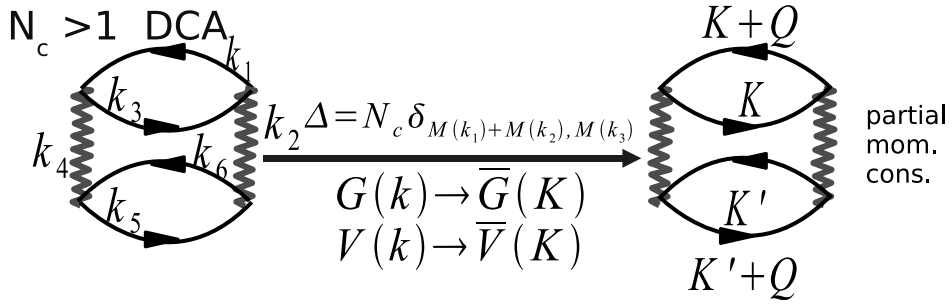

FIGURE 8. A second-order term in the generating functional of the Hubbard model. Here the undulating line represents the interaction U, and on the LHS (RHS) the solid line the lattice (coarse-grained) single-particle Green functions. When the DCA Laue function is used to describe momentum conservation at the internal vertices, the momenta collapse onto the cluster momenta and each lattice Green function is replaced by the coarse-grained result.

This is illustrated for the second-order term in the generating functional in Fig. 8. Each internal leg $G(\mathbf{k})$ in a diagram is replaced by the coarse–grained Green function $\bar{G}(\mathbf{M}(\mathbf{k}))$, defined by

$$\bar{G}(\mathbf{K}) \equiv \frac{N_c}{N} \sum_{\tilde{\mathbf{k}}} G(\mathbf{K} + \tilde{\mathbf{k}}) \quad , \tag{6}$$

where N is the number of points of the lattice, N_c is the number of cluster $\mathbf{K}$ points, and the $\tilde{\mathbf{k}}$ summation runs over the momenta of the cell about the cluster momentum $\mathbf{K}$ (see, Fig. 7). The diagrammatic sequences for the generating functional and its functional derivatives are unchanged; however, the complexity of the problem is greatly reduced since $N_c \ll N$.

As with the DMFA, the coarse-graining approximation will be applied to only the compact part of the free energy, Φ, and its functional derivatives. Physically, this is justified by the fact that irreducible terms like the self energy are short ranged, while reducible quantities the G must be able to long length and time scale physics. This is motivated in Fig. 9. As the particle propagates from the origin to space-time location x, the quantum phase and amplitude it accumulates is descripbed by the single-particle Green function $G(x)$. Consequently if x is larger than the size of the DCA cluster, then $G(x)$ is poorly approximated by the cluster Green function. However, the Self energy Σ describes the many-body processes that produce the screening cloud surrounding the particle. These processes are generally short ranged in a strongly correlated many-body system, so the self energy is often well approximated by the cluster quantity. Formally,

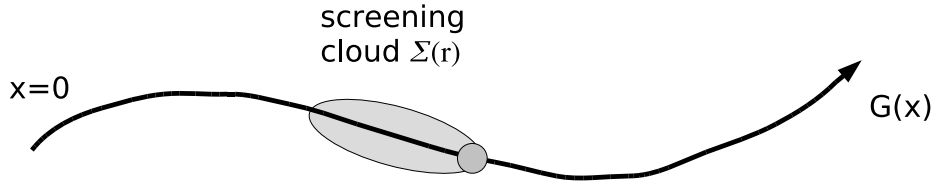

FIGURE 9. Screening of a propagating particle. The single particle green function, which describes the quantum phase and amplitude the particle accumulates, is poorly approximated by a small cluster calculation. Its self energy, which describes generally short ranged screening processes, is well approximated by a small cluster calculation.

we have justified this elsewhere by exploring the Δk-dependence of the compact and non-compact parts of the free energy[16]. The generating functional is the sum over all of the closed connected compact diagrams, such as the one shown in Fig. 8. The corresponding DCA estimate for the free energy is

$$F_{DCA} = -k_B T \left(\Phi_c - \mathrm{Tr}\left[\Sigma_\sigma G_\sigma\right] - \mathrm{Tr}\ln\left[-G_\sigma\right]\right) \tag{7}$$

where Φ_c is the cluster generating functional. The trace indicates summation over frequency, momentum and spin. F_{DCA} is stationary with respect to $\mathbf{G}_\sigma$,

$$\frac{-1}{k_B T}\frac{\delta F_{DCA}}{\delta G_\sigma(\mathbf{k})} = \Sigma_{c\sigma}(M(\mathbf{k})) - \Sigma_\sigma(\mathbf{k}) = 0, \tag{8}$$

which means that $\Sigma(\mathbf{k}) = \Sigma_{c\sigma}(M(\mathbf{k}))$ is the proper approximation for the lattice self energy corresponding to Φ_c. The corresponding lattice single-particle propagator is then given by

$$G(\mathbf{k}, z) = \frac{1}{z - \varepsilon_{\mathbf{k}} - \varepsilon - \Sigma_c(M(\mathbf{k}), z)}. \tag{9}$$

A similar procedure is used to construct the two-particle quantities needed to determine the phase diagram or the nature of the dominant fluctuations that can eventually

destroy the quasi-particle. This procedure is a generalization of the method of calculating response functions in the DMFA[17, 18]. In the DCA, the introduction of the momentum dependence in the self-energy will allow one to detect some precursor to transitions which are absent in the DMFA; but for the actual determination of the nature of the instability, one needs to compute the response functions. These susceptibilities are thermodynamically defined as second derivatives of the free energy with respect to external fields. $\Phi_c(G)$ and $\Sigma_{c\sigma}$, and hence F_{DCA} depend on these fields only through G_σ and G^0_σ. Following Baym[19] it is easy to verify that, the approximation

$$\Gamma_{\sigma,\sigma'} \approx \Gamma_{c\sigma,\sigma'} \equiv \delta\Sigma_{c\sigma}/\delta G_{\sigma'} \tag{10}$$

yields the same estimate that would be obtained from the second derivative of F_{DCA} with respect to the applied field. For example, the first derivative of the free energy with respect to a spatially homogeneous external magnetic field h is the magnetization,

$$m = \mathrm{Tr}\left[\sigma G_\sigma\right]. \tag{11}$$

The susceptibility is given by the second derivative,

$$\frac{\partial m}{\partial h} = \mathrm{Tr}\left[\sigma \frac{\partial G_\sigma}{\partial h}\right]. \tag{12}$$

We substitute $G_\sigma = \left(G^{0-1}_\sigma - \Sigma_{c\sigma}\right)^{-1}$, and evaluate the derivative,

$$\frac{\partial m}{\partial h} = \mathrm{Tr}\left[\sigma \frac{\partial G_\sigma}{\partial h}\right] = \mathrm{Tr}\left[G^2_\sigma\left(1 + \sigma \frac{\partial \Sigma_{c\sigma}}{\partial G_{\sigma'}}\frac{\partial G_{\sigma'}}{\partial h}\right)\right]. \tag{13}$$

If we identify $\chi_{\sigma,\sigma'} = \sigma\frac{\partial G_{\sigma'}}{\partial h}$, and $\chi^0_\sigma = G^2_\sigma$, collect all of the terms within both traces, and sum over the cell momenta $\tilde{\mathbf{k}}$, we obtain the two–particle Dyson's equation

$$\begin{aligned} 2\left(\bar{\chi}_{\sigma,\sigma} \;&-\; \bar{\chi}_{\sigma,-\sigma}\right) \\ &= \; 2\bar{\chi}^0_\sigma + 2\bar{\chi}^0_\sigma\left(\Gamma_{c\sigma,\sigma} - \Gamma_{c\sigma,-\sigma}\right)\left(\bar{\chi}_{\sigma,\sigma} - \bar{\chi}_{\sigma,-\sigma}\right). \end{aligned} \tag{14}$$

We see that again it is the irreducible quantity, i.e. the vertex function, for which cluster and lattice correspond.

3.3. Cluster Selection

The geometry of the DCA cluster is relevant for systematic studies of phase transitions. All cluster geometries which can be used to tile the lattice without gaps are valid (c.f. Fig. 10). In this approximation, the lattice has long ranged order once the correlation length ξ of the order reaches the linear cluster size, since then the lattice tiled with such clusters would be ordered. A scaling Ansatz for T_c which captures these ideas is[20]

$$\xi\left(T_c(N_c)\right) = N_c^{1/D} \tag{15}$$

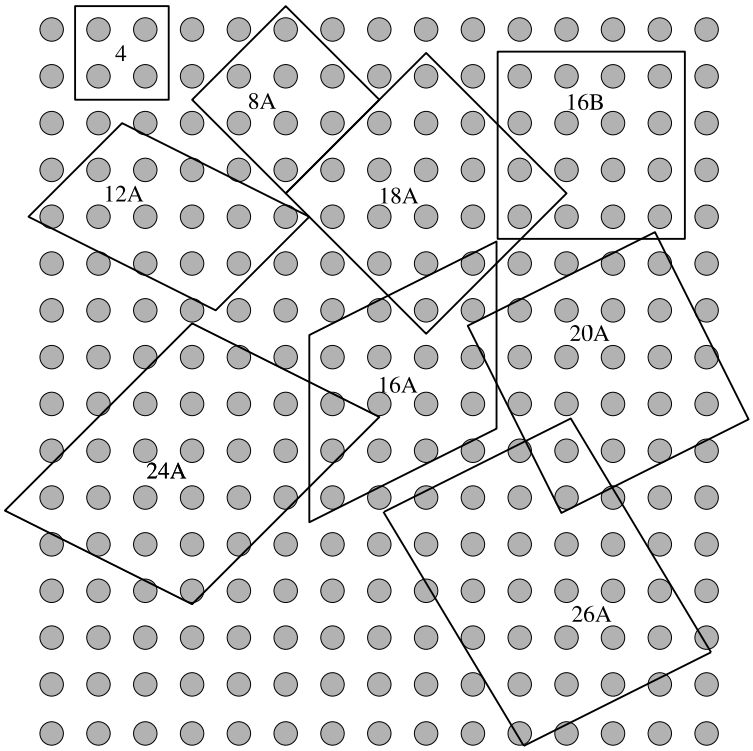

FIGURE 10. A variety of cluster geometries which may be used to tile a two-dimensional square lattice.

. So for a typical transition, with $\xi(T) \propto |T - T_c^*|^{-\nu}$ (where T_c^* is the transition temperature of the thermodynamic lattice), the scaling formula is $T_c^* = T_c(N_c) - A(N_c)^{-1/D\nu}$, where A, ν, and T_c^* are fit to the data $T_c(N_c)$. However, clearly this approach will not apply to clusters with strange geometries, like e.g. rods in a 2D system.

Ideal clusters should properly represent all length scales upto $N_c^{1/D}$, and no others. Consider the 16-site clusters show in Fig. 11, the number of neighbors in each neighbor shell are shown in the adjacent tables.[21] On the lattice, the nth shell has 4n neighbors. Both 16A and 16B have complete near neighbor (n=1) shells with four near neighbors. However, the conventional square cluster 16B, has 6 (not 8) sites in the n=2 shell, has 4 (not 12) in the n=3 shell, and even on site in the n=4 shell. The cluster 16A is far better, with no site in the n=4 shell and a nearly complete n=2 shell.

Betts explored different cluster geometries, and realized that there are few clusters with the same geometry (point group) as the lattice, but far more with lower symmetry that are often superior. He selected for neighbors in a given shell, symmetry, and squareness. Since for a given cluster size, one incomplete shell is usually inevitable, he classified the imperfection of cluster by the number of missing sites in smaller shell than the incomplete one and the number of additional sites in larger shells. Thus, 16B has in imperfection of three while 16A has an imperfection of one. The imperfection number is the most important selection criteria.

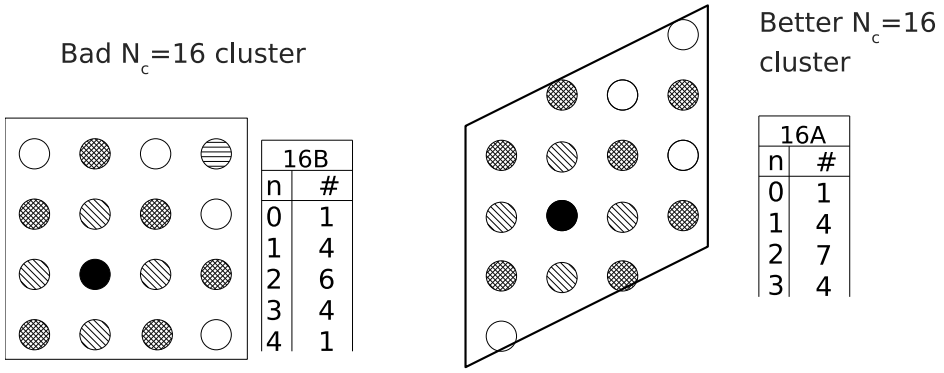

FIGURE 11. Two sixteen ($N_c = 16$ site periodic clusters. Here, the neighbors to the black site are shown in different colors. Near-neighbors are blue, next near neighbors are green, next-next neighbors red, etc.

4. CALCULATION OF PHYSICAL PROPERTIES

Most experiments measure quantities which we can express theoretically as reducible one or two-particle green functions. As discussed above, the appropriate way to calculate these quantities is to first extract the corresponding irreducible quantity from the cluster calculation, and then use it to calculate the reducible quantity. For example, to calculate the single-particle Green function (relevant for angle-resolved photoemission spectroscopy) we first extract the cluster self energy and use the Dyson equation to construct the lattice Green function. To calculate the phase diagram, we calculate the irreducible vertices in the different scattering channels Γ, and insert them into the Bethe-Salpeter equations for the lattice. In this subsection we will provide more details about the relationship between the lattice and cluster two-particle Green functions and describe how a lattice susceptibility may be calculated efficiently.

4.0.1. Particle-hole channel

As a specific example, we will describe the calculation of the two-particle Green function

$$\begin{aligned}\chi_{\sigma,\sigma'}(q,k,k') &= \int_0^\beta\int_0^\beta\int_0^\beta\int_0^\beta d\tau_1 d\tau_2 d\tau_3 d\tau_4 \\ &\times\ e^{i\left((\omega_n+\nu)\tau_1-\omega_n\tau_2+\omega_{n'}\tau_3-(\omega_{n'}+\nu)\tau_4\right)} \\ &\times\ \langle T_\tau c^\dagger_{\mathbf{k}+\mathbf{q}\sigma}(\tau_1)c_{\mathbf{k}\sigma}(\tau_2)c^\dagger_{\mathbf{k}'\sigma'}(\tau_3)c_{\mathbf{k}'+\mathbf{q}\sigma'}(\tau_4)\rangle \quad ,\end{aligned}$$

where we adopt the conventional notation [22] $k = (\mathbf{k}, i\omega_n)$, $k' = (\mathbf{k}, \omega'_n)$, $q = (\mathbf{q}, \nu_n)$ and T_τ is the time ordering operator.

$\chi_{\sigma,\sigma'}(q,k,k')$ and $\Gamma_{\sigma,\sigma'}(q,k,k')$ are related to each other through the Bethe-Salpeter equation:

$$\chi_{\sigma,\sigma'}(q,k,k') = \chi^0_{\sigma,\sigma'}(q,k,k') + \chi^0_{\sigma,\sigma''}(q,k,k'')$$

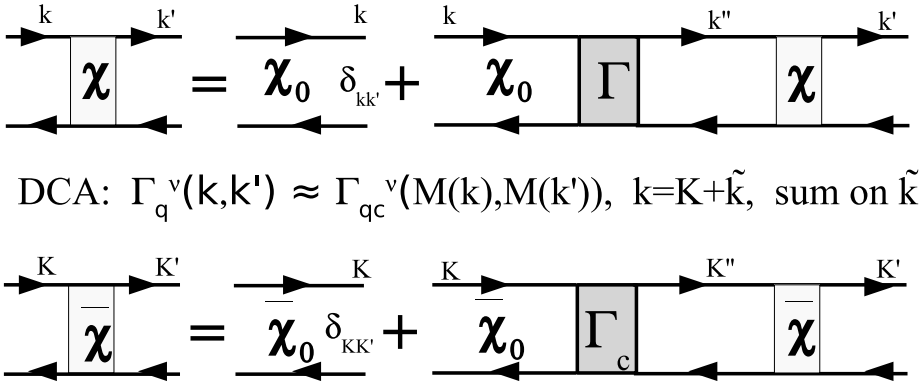

FIGURE 12. The Beth-Salpeter equation in the DCA. We approximate the lattice irreducible vertex Γ^{ν} by the Γ_c^{ν} from the DCA cluster and coarse-grain over the $\tilde{\mathbf{k}}$. The remaining equation is a function of the cluster $\mathbf{K}$ only and may be solved by inversion.

$$\times \quad \Gamma_{\sigma'',\sigma'''}(q,k'',k''')\chi_{\sigma''',\sigma'}(q,k''',k') \tag{16}$$

where $\Gamma_{\sigma,\sigma'}(q,k,k')$ is the two-particle irreducible vertex which is the analogue of the self-energy, $\chi^0_{\sigma,\sigma'}(q,k,k'')$ is the non-interacting susceptibility constructed from a pair of fully-dressed single-particle Green functions. As usual, a summation is to be made for repeated indices.

We now make the DCA substitution $\Gamma_{\sigma,\sigma'}(\mathbf{q},\mathbf{k},\mathbf{k}') \rightarrow \Gamma_{c\sigma,\sigma'}(\mathbf{q},\mathbf{M}(\mathbf{k}),\mathbf{M}(\mathbf{k}'))$ in Eq. 16 (where frequency labels have been suppressed). Note that only the bare and dressed two-particle Green functions χ depend upon the momenta $\tilde{\mathbf{k}}$ within a cell. Since χ and χ^0 in the product on the RHS of Eq. 16 share no common momentum labels, we may freely sum over the momenta $\tilde{\mathbf{k}}$ within a cell, yielding

$$\begin{aligned}\bar{\chi}_{\sigma,\sigma'}(q,K,K') &= \bar{\chi}^0_{\sigma,\sigma'}(q,K,K') + \bar{\chi}^0_{\sigma,\sigma''}(q,K,K'') \\ &\times \quad \Gamma_{c\sigma'',\sigma'''}(q,K'',K''')\bar{\chi}_{\sigma''',\sigma'}(q,K''',K')\,. \end{aligned} \tag{17}$$

By coarse-graining the Bethe-Salpeter equation, we have greatly reduced its complexity; each of the matrices above is sufficiently small that they may be easily manipulated using standard techniques.

In contrast with the single-particle case where the coarse-grained quantities are identical to those of the cluster, $\chi_{c\sigma,\sigma'}(q,K,K')$ is not equal to $\bar{\chi}_{\sigma,\sigma'}(q,K,K')$. This is because the self-consistency is made only at the single-particle level. Unlike the single particle case where both $\Sigma(K)$ and $\bar{G}(K)$ are directly calculated, neither $\Gamma_{\sigma,\sigma'}(q,K,K')$ nor the coarse-grained susceptibility $\bar{\chi}_{\sigma,\sigma'}(q,K,K')$ are calculated during the self-consistency. Instead, the coarse-grained non-interacting susceptibility $\bar{\chi}^0_{\sigma,\sigma'}(q,K,K')$ is calculated in a separate program after the DCA converges using the following relation

$$\begin{aligned}\bar{\chi}^0_{\sigma,\sigma'}[(\mathbf{q},i\nu_n);(\mathbf{K},i\omega_n);(\mathbf{K}',i\omega'_n)] &= \delta_{\sigma,\sigma'}\delta_{\mathbf{K},\mathbf{K}'}\delta_{\omega_n,\omega'_n} \\ \times\frac{N_c}{N}\sum_{\tilde{\mathbf{k}}} G_\sigma(\mathbf{K}+\tilde{\mathbf{k}},i\omega_n)G_\sigma(\mathbf{K}+\tilde{\mathbf{k}}+\mathbf{q},i\omega_n+\nu_n) \quad .\end{aligned} \tag{18}$$

The corresponding cluster susceptibility is calculated by the cluster solver and the vertex function is extracted by inverting the cluster two-particle Bethe-Salpeter equation

$$\chi_{c\sigma,\sigma'}(q,K,K') = \chi^0_{c\sigma,\sigma'}(q,K,K') + \chi^0_{c\sigma,\sigma''}(q,K,K'') \times\Gamma_{c\sigma'',\sigma'''}(q,K'',K''')\chi_{c\sigma''',\sigma'}(q,K''',K') \,. \tag{19}$$

If we combine Eqs. 19 and 17, then the coarse-grained susceptibility may be obtained after elimination of $\Gamma(q,K,K')$ between the two equations. It reads

$$\bar{\chi}^{-1} = \chi_c^{-1} - \chi_c^{0^{-1}} + \bar{\chi}^{0^{-1}} \,, \tag{20}$$

where, for example, $\bar{\chi}$ is the matrix formed from $\bar{\chi}_{\sigma,\sigma'}(q,K,K')$ for fixed q. The charge (ch) and spin (sp) susceptibilities $\chi_{ch,sp}(q,T)$ are deduced from $\bar{\chi}$

$$\chi_{ch,sp}(q,T) = \frac{(k_B T)^2}{N_c^2} \sum_{KK'\sigma\sigma'} \lambda_{\sigma\sigma'}\bar{\chi}_{\sigma,\sigma'}(q,K,K') \quad , \tag{21}$$

where $\lambda_{\sigma\sigma'} = 1$ for the charge channel and $\lambda_{\sigma\sigma'} = \sigma\sigma'$ for the spin channel.

4.0.2. Particle-particle channel

The calculation of susceptibilities in the particle-particle channel is essentially identical to the above. The exception to this rule occurs when we calculate susceptibilities for transitions to states of lower symmetry than the lattice symmetry. For example, in order to obtain the pair function of the desired symmetry (s,p,d), the two-particle Green function must be multiplied by the corresponding form factors $g(\mathbf{k})$ and $g(\mathbf{k}')$. In the study of the Hubbard model below, we will be particularly interested in $g(\mathbf{k}) = 1$ (s wave), $g(\mathbf{k}) = cos(k_x) + cos(k_y)$ (extended s wave) and $g(\mathbf{k}) = cos(k_x) - cos(k_y)$ ($d_{x^2-y^2}$ wave). These symmetries have been evoked as possible candidates for the superconducting ground state.

These factors modify the Bethe-Salpeter equations

$$\begin{aligned} g(\mathbf{k})\chi(q,k,k')g(\mathbf{k}') &= g(\mathbf{k})\chi^0(q,k,k')g(\mathbf{k}') \\ &+ \quad g(\mathbf{k})\chi^0(q,k,k'') \times \Gamma(q,k'',k''') \times \chi(q,k''',k')g(\mathbf{k}') \end{aligned} \tag{22}$$

where

$$\begin{aligned} \chi(q,k,k') \quad &= \quad \int_0^\beta \int_0^\beta \int_0^\beta \int_0^\beta d\tau_1 d\tau_2 d\tau_3 d\tau_4 \\ &\times \quad e^{i\left((\omega_n+\nu)\tau_1 - \omega_n\tau_2 + \omega_{n'}\tau_3 - (\omega_{n'}+\nu)\tau_4\right)} \\ &\times \quad \langle T_\tau c^\dagger_{\mathbf{k}+\mathbf{q}\sigma}(\tau_1) c^\dagger_{-\mathbf{k}-\sigma}(\tau_2) c_{-\mathbf{k}'-\sigma}(\tau_3) c_{\mathbf{k}'+\mathbf{q}\sigma}(\tau_4)\rangle \quad , \end{aligned} \tag{23}$$

On the LHS, we have dropped the spin indices since we will consider only opposite-spin pairing. Eq. 22 cannot be easily solved if it is coarse-grained, since this will partially

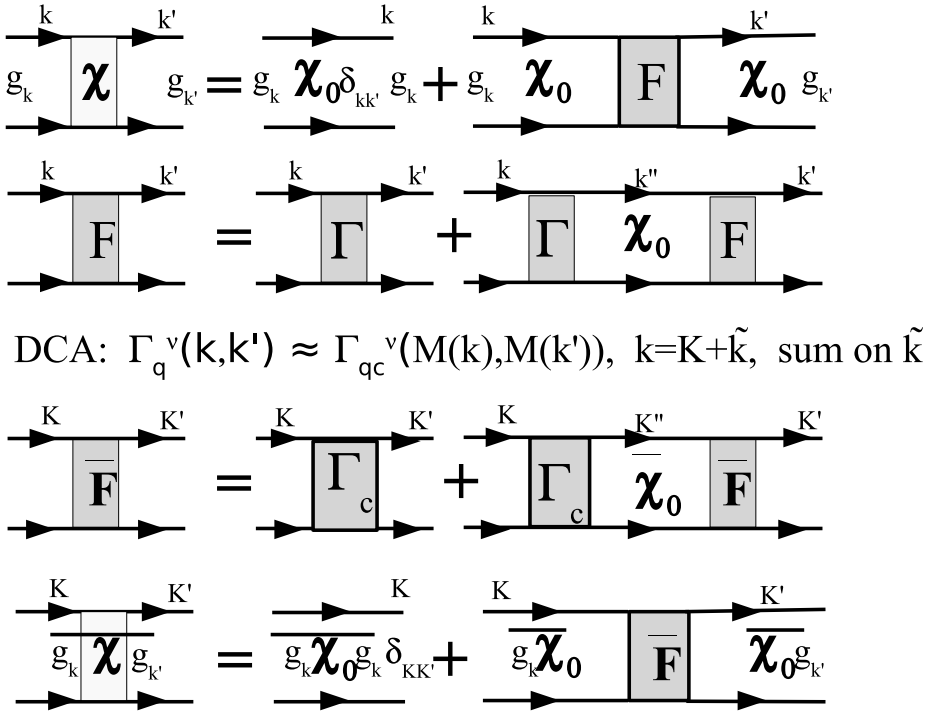

FIGURE 13. Calculation of particle-particle projected susceptibilities. Often we want to calculate a projected particle-particle susceptibility (e.g. d-wave, with $g_{\mathbf{k}} = \cos(k_x) - \cos(k_y)$). Here the Bethe-Salpeter equation is rewritten in terms of the irreducible vertex F. We approximate the lattice irreducible vertex Γ^ν by the Γ_c^ν from the DCA cluster and coarse-grain over the $\tilde{\mathbf{k}}$. Then the projected bare bubbles are calculated, and the remaining equation is a function of the cluster $\mathbf{K}$ only and may be solved by inversion.

convolve $\chi(q,k,k')$ with *two* factors of g on the LHS and *one* factor on the RHS. Hence for the pairing susceptibilities, or for any situation where non-trivial form factors must be used, we use the equivalent equation involving the reducible vertex F (instead of the irreducible vertex Γ)

$$\begin{aligned} g(\mathbf{k})\chi(q,k,k')g(\mathbf{k}') &= g(\mathbf{k})\chi^0(q,k,k')g(\mathbf{k}') \\ &+ g(\mathbf{k})\chi^0(q,k,k'') \\ &\times F(q,k'',k''')\chi^0(q,k''',k')g(\mathbf{k}'), \end{aligned} \tag{24}$$

where

$$\begin{aligned} F(q,k,k') &= \Gamma(q,k,k') \\ &+ \chi^0(q,k,k'')\Gamma(q,k'',k''')\chi^0(q,k''',k') + \cdots \end{aligned} \tag{25}$$

We define

$$\Pi_{g,g}(q,k,k') = g(\mathbf{k})\chi(q,k,k')g(\mathbf{k}') \tag{26}$$

$$\Pi^0_{g,g}(q,k,k') = g(\mathbf{k})\chi^0(q,k,k')g(\mathbf{k}') \quad (27)$$

$$\Pi^0_{g}(q,k,k') = g(\mathbf{k})\chi^0(q,k,k')\,. \quad (28)$$

The remaining steps of the calculation are similar to the particle-hole case. We invert the cluster particle-particle Bethe-Salpeter equation with $g = 1$ for the cluster, in order to extract Γ_c. We then coarse-grain Eq. 25, and use Γ_c to calculate the coarse-grained $\bar{F} = \Gamma_c \left(1 - \bar{\chi}^0 \Gamma_c\right)^{-1}$. We then coarse-grain Eq. 24, and use the coarse-grained $\bar{F}$ to calculate the coarse-grained $\bar{\Pi}_{g,g}$

$$\begin{aligned} \bar{\Pi}_{g,g}(q,K,K') &= \bar{\Pi}^0_{g,g}(q,K,K') \\ &+ \bar{\Pi}^0_{g}(q,K,K'')\bar{T}_2(q,K'',K''')\bar{\Pi}^0_{g}(q,K''',K')\,. \end{aligned} \quad (29)$$

The pairing susceptibility of a desired symmetry is given by

$$P_g(q,T) = \frac{(k_B T)^2}{N_c^2} \sum_{K,K'} \bar{\Pi}_{gg}(q,K,K') \quad . \quad (30)$$

5. CONCLUSION

Coarse-graining methods are used to derive the DMFA, and DCA which map the lattice onto a self-consistently embedded cluster problem. The DMFA is a local approximation, while the DCA incorporates systematic non-local corrections. Irreducible quantities from the cluster are used to calculate reducible lattice quantities.

We would like to acknowledge useful conversations and fruitful collaborations with B. Goodman, M. Hettler, H. R. Krishnamurthy, M. Ma, Th. Maier, R. Scalettar, Th. Pruschke, and F.C. Zhang. This work was supported by the National Science Foundation grants DMR-0706379 and DMR-0312680.

REFERENCES

1. J. Hubbard, Proc. R. Soc. a**276**, 238(1963); M.C. Gutzwiller, Phys. Rev. Lett. **10**, 159(1963); J. Kanamori, Prog. Theor. Phys. **30**, 257(1963).
2. Proceedings of the international conference on "Itinerant-Electron Magnetism". Physica B+C**91** (1977); for a review about the theory of the Hubbard model see also D. Vollhardt, Rev. Mod. Phys. 56, 99(1984).
3. E.H. Lieb and F.Y. Wu, Phys. Rev. Lett. **20**, 1445 (1968); H. Frahm and V.E. Korepin, Phys. Rev. B**42**, 10533(1990); N. Kawakami and S.-K. Yang, Phys. Rev. Lett. **65**, 2309(1990).
4. G. Czycholl, J. Mag. Mag. Mat. **47,48**, 350 (1985).
5. W. Metzner and D Vollhardt, Phys. Rev. Lett. **62**, 324 (1989).
6. E. Müller-Hartmann, Z. Phys. B **74**, 507 (1989).
7. P.G.J. van Dongen and D. Vollhardt, Phys. Rev. Lett. **65**, 1663 (1990).
8. M.H. Hettler, A.N. Tahvildar-Zadeh, M. Jarrell, T. Pruschke, and H.R. Krishnamurthy, Phys. Rev. **B 58,** 7475 (1998).
9. M. H. Hettler, M. Mukherjee, M. Jarrell, and H.R. Krishnamurthy, Phys. Rev. B 61, 12739 (2000).
10. C. Kim, Y. Kuramoto and T. Kasuya, J. Phys. Soc. Japan **59**, 2414(1990).
11. T. Pruschke, M. Jarrell and J.K. Freericks, Adv. in Phys. **42,** 187 (1995).

12. A. Georges, G. Kotliar, W. Krauth and M.J. Rozenberg, Rev. Mod. Phys. **68,** 13 (1996).
13. R.M. Fye and J.E. Hirsch, Phys. Rev. B **38**, 433 (1988).
14. M. Jarrell, Th. Maier, C. Huscroft, and S. Moukouri, Phys. Rev. B 64, 195130/1-23 (2001).
15. M. Jarrell, and J.E. Gubernatis, Physics Reports Vol. **269** #3, (1996).
16. K. Aryanpour, M.H. Hettler and M. Jarrell, Phys. Rev. B 65, 153102/1-4 (2002).
17. V. Zlatić and B. Horvatić, Sol. St. Comm. **75**, 263 (1990).
18. M. Jarrell, Phys. Rev. Lett. **69**, 168(1992)
19. G. Baym and L.P. Kadanoff, Phys. Rev. **124**, 287, (1961).
20. Kent, P; Jarrell, M; Maier, T; Pruschke, T. Phys. Rev. B 72, 060411 (2005).
21. D. D. Betts, H. Q. Lin, and J. S. Flynn, Can. J. Phys. 77, 353 (1999); D. D. Betts and G. E. Stewart, Can. J. Phys. 75, 47 (1997).
22. A.A. Abrikosov, L.P. Gorkov, I.E. Dzyalishinski, *Methods of Quantum Field Theory in Statistical Physics*, (Dover, New York, 1975).